Towards a Quantitative Theory of Epidermal Calcium Profile Formation in Unwounded Skin

Matthew P. Adams[1,*], Daniel G. Mallet[2], Graeme J. Pettet[2]

1 Mathematical Sciences School and Institute of Health and Biomedical Innovation, Queensland University of Technology, Brisbane, Queensland, Australia, and School of Chemical Engineering, The University of Queensland, Brisbane, Queensland, Australia
2 Mathematical Sciences School and Institute of Health and Biomedical Innovation, Queensland University of Technology, Brisbane, Queensland, Australia
∗ E-mail: mp.adams@qut.edu.au

Abstract

We propose and mathematically examine a theory of calcium profile formation in unwounded mammalian epidermis based on: changes in keratinocyte proliferation, fluid and calcium exchange with the extracellular fluid during these cells' passage through the epidermal sublayers, and the barrier functions of both the stratum corneum and tight junctions localised in the stratum granulosum. Using this theory, we develop a mathematical model that predicts epidermal sublayer transit times, partitioning of the epidermal calcium gradient between intracellular and extracellular domains, and the permeability of the tight junction barrier to calcium ions. Comparison of our model's predictions of epidermal transit times with experimental data indicates that keratinocytes lose at least 87% of their volume during their disintegration to become corneocytes. Intracellular calcium is suggested as the main contributor to the epidermal calcium gradient, with its distribution actively regulated by a phenotypic switch in calcium exchange between keratinocytes and extracellular fluid present at the boundary between the stratum spinosum and the stratum granulosum. Formation of the extracellular calcium distribution, which rises in concentration through the stratum granulosum towards the skin surface, is attributed to a tight junction barrier in this sublayer possessing permeability to calcium ions that is less than $15\,\mathrm{nm\,s^{-1}}$ in human epidermis and less than $37\,\mathrm{nm\,s^{-1}}$ in murine epidermis. Future experimental work may refine the presented theory and reduce the mathematical uncertainty present in the model predictions.

Introduction

The calcium distribution within the mammalian epidermis is both an indicator of the skin barrier function [1] and a regulator of epidermal structure [2]. Here, using a mathematical model, we propose and examine a theory of the key mechanisms that control the calcium profile in unwounded epidermis.

The epidermis and its calcium profile

The epidermis consists predominantly of keratinocytes [3]. These cells are continuously being produced at the bottom of the epidermis, driven to passively migrate towards the skin surface, and are sloughed away during everyday activity [4]. During this life cycle, keratinocytes express distinct phenotypic changes which characterise the boundaries of four sublayers of the epidermis:

1. The *stratum basale* (SB): Keratinocytes proliferate. The exact pattern of proliferation is still a matter of debate [5], and is suggested to involve either one [6, 7] or two cell types [8]. The single progenitor theory posits that a single population of slowly-cycling cells maintains epidermal homeostasis, whilst the more traditional two progenitor theory proposes that the SB consists of two keratinocyte subpopulations: (1) stem cells, which proliferate slowly and indefinitely, each time producing one stem cell and one transit amplifying (TA) cell, and (2) TA cells, which divide symmetrically 3-5 times before leaving the SB [9, 10].

2. The *stratum spinosum* (SS): Keratinocytes increase in volume [11] and passively migrate towards the skin surface, displaced from the SB by proliferation there.

3. The *stratum granulosum* (SG): Keratinocytes become flattened and disintegrate, reducing their volume [12] and expelling lamellar bodies [13].

4. The *stratum corneum* (SC): Denucleated and highly flattened keratinocytes, called corneocytes, combine with lipids from the lamellar bodies exocytosed in the SG, in a "bricks and mortar" architecture [14] that forms the primary skin barrier [4]. Transepidermal water loss (TEWL) experiments, which involve progressive tape-stripping of the SC to identify the thickness that must be removed to cause fluid flow to significantly increase across this sublayer, suggest that this barrier is only strongly impermeable in the top 4-8 μm of the SC [15–17]. Hence we subdivide this epidermal sublayer into the *lower SC* (progressive barrier) and *upper SC* (impermeable barrier). At the top of the upper SC, intercorneocyte linking structures degrade and corneocytes are shed from the skin surface [18].

Epidermal calcium is present in three different localisations: the extracellular fluid (ECF), intracellular cytosol and intracellular organelles [19]. Calcium concentrations in the ECF and organelles are significantly higher than in the cytosol [20, 21]. These concentration differences are maintained by calcium pumps present on the membranes of keratinocytes and their intracellular structures, which actively remove calcium from the cytosol [22]. If we consider calcium in the ECF as "extracellular", and calcium in cytosol and organelles together as "intracellular", then it is the action of the calcium pumps on the keratinocyte membrane that is crucial for controlling intracellular and extracellular calcium levels [23].

The total epidermal calcium profile, which is a summation of calcium from intracellular and extracellular localisations, has been quantitatively measured using proton-induced X-ray emission (PIXE) [24–28], and in unwounded skin these measurements typically adhere to the profile shown in Figure 1a. The total calcium concentration is low in the SB, rises gradually to a peak in the SG (the so-called "epidermal calcium gradient"), and drops to near-negligible levels in the SC. Because the PIXE technique has a resolution of $\sim$10 μm [29], it is unclear whether the calcium drop towards the skin surface occurs at the SG-SC interface or further into the SC: the latter interpretation is quite feasible since the skin's primary barrier might only be fully formed in the upper SC, based on the previously discussed TEWL experiments. PIXE cannot distinguish between the intracellular and extracellular contributions to the epidermal calcium profile.

On the other hand, the intracellular and extracellular epidermal calcium profiles have been measured separately using ion capture cytochemistry [30,31], but only semi-quantitatively [32–34]. As indicated in Figure 1b, both intracellular and extracellular profiles qualitatively agree with the total profiles obtained from PIXE, but it is difficult to make additional interpretations from this semi-quantitative data.

For the past decade, the presence of the epidermal calcium profile has been attributed solely to the presence of the SC barrier [35], which is thought to act as a sieve, selectively allowing water but not calcium to leave the viable epidermis [36]. When the epidermis is wounded, its calcium profile disappears rapidly then reappears gradually with restoration of the skin's barrier function [1,37,38]. This observation fits easily within the conventional sieve view of epidermal calcium profile formation, as the removal of the SC simply removes the impetus for the calcium gradient to form.

However, recent measurements of the epidermal calcium distribution using fluorescent lifetime imaging [36, 39] have brought this view into question. These measurements demonstrated that the bulk of free calcium is present in intracellular organelles [36], and that epidermal barrier disruption triggers a mobilization of high amounts of calcium from these stores [39]. This prompted the questioning of this conventional view that the epidermal calcium profile is regulated only passively by the SC. In previous work, using a mathematical model, we found that this profile is largely intracellular and regulated by sublayer-specific changes in the action of keratinocyte membrane pumps [23]. In the current paper, we extend this analysis further, to propose that there are three key mechanisms that control epidermal calcium

profile formation in unwounded skin: the passive impermeable barrier of the SC, tight junction-limited calcium diffusion in the SG, and a phenotypic switch in calcium exchange between keratinocytes and extracellular fluid at the SS-SG boundary. We also investigate the contribution of the stem and TA cell subpopulations of the SB, volume changes of keratinocytes in the SS, and calcium located in the lower SC, to the formation of the calcium profile of unwounded epidermis.

Proposed key mechanisms regulating the calcium profile

Our proposed theory is presented schematically in Figure 2. We treat the calcium present in the cytosol and organelles within keratinocytes together as intracellular calcium, with the majority of this calcium likely to be confined to the keratinocyte organelles [21]. Most epidermal calcium is present in this intracellular calcium [36], which possesses a distinct spatial profile that forms as follows. Membrane pumps on keratinocytes act to accumulate calcium intracellularly from the ECF in the SB and SS, and in the SG this behaviour reverses to calcium expulsion into the ECF [23], emptying the intracellular stores [39] so that corneocytes in the upper SC contain negligible levels of intracellular calcium. These mechanisms yield an intracellular calcium profile that is low in the SB, rises gradually towards a peak in the SG, and drops rapidly in the SC, in agreement with the experimental observations for both the total and intracellular profiles (see Figures 1a and 1b).

The extracellular calcium profile, which possesses far less calcium due to the small volume of the epidermis occupied by the ECF [36, 40], forms as follows. The ECF is essentially water [41], and hence extracellular calcium in the SB and SS diffuses rapidly to near-constant levels throughout these sublayers [23]. In the SG, cell-cell adhesions known as tight junctions (TJs) are located apically between the lateral membranes of neighbouring keratinocytes [42, 43], and form a permeability barrier to calcium ions [44, 45] that reduces the rate of extracellular calcium diffusion there. Because calcium is continuously being expelled by keratinocytes near the skin surface, this TJ-limited calcium diffusion in the SG causes the extracellular calcium concentration to be slightly elevated there, negligibly affecting the calcium levels in the underlying SB and SS [46]. Lipids cannot be responsible for this elevated extracellular calcium concentration in the SG because they are localised only at the SG-SC boundary prior to their contribution as the "mortar" of the SC barrier. Extracellular calcium cannot enter the upper SC due to its barrier function, in agreement with the TEWL experiments [15–17]. These mechanisms together yield an extracellular calcium profile which is nearly constant in the SB and SS, rises in the SG, and drops rapidly in the SC, in agreement with experimental observations of the extracellular profile (see Figure 1b).

Materials and Methods

Main equations

We mathematically model the epidermis as a saturated porous medium [47]. This modelling strategy has been used previously to consider avascular tumour growth [48-50] and cell behaviour within an artificial scafffold [51], justified for the viable sublayers of the epidermis in our previous paper [23], and proposed for modelling the SC of the epidermis by Kitson and Thewalt [52].

As a porous medium, we assume that the keratinocytes behave uniformly and are analogous to soil particles, and the surrounding ECF is analogous to the water that saturates the soil system. We assume that keratinocytes and ECF are comprised of an identical, incompressible fluid. Calcium is always dissolved in the cells or ECF. Calcium contained in the cytosol and intracellular organelles of cells are considered together simply as intracellular calcium. This simplification means that we do not specifically consider the intracellular dynamics of calcium exchange between the cytosol and organelles. We cannot discount the possibility that the intracellular calcium dynamics may play an important role in

the partitioning of calcium between intracellular and extracellular domains, although investigating this is beyond the scope of the present work. As we are only interested here in identifying the extracellular and intracellular contributions to the epidermal calcium profile, consideration of cytosolic and organelle calcium separately is not necessary to investigate our proposed theory. Experimentally, intracellular calcium waves are known to propagate between adjacent keratinocytes [53], but these waves negligibly affect the epidermal calcium profile. Hence, in our model calcium cannot travel directly between keratinocytes, but rather can only be exchanged between cells and the surrounding ECF.

We assume that both the structure and calcium profile of the epidermis have reached a distribution that is stable and unchanging with time. Because of this we consider only one spatial direction z perpendicular to the skin surface. For this simplification, we ensured that any model parameters recorded for the three-dimensional case are also appropriate for the one-dimensional case. The main equations of our model, derived from mass conservation equations for the fluid and calcium present both in cells and ECF, are identical to those from our previous paper [23], but with one important exception. We do not specify the ECF velocity, because it will be unpredictably modified by TJs [54] and aquaporins [55, 56], neither of which were considered in [23]. With all these considerations in mind, the main equations of our model are

$$\frac{\mathrm{d}}{\mathrm{d}z}\left(\phi u_i\right) = f,\tag{1a}$$

$$\frac{\mathrm{d}}{\mathrm{d}z}\left(\rho_{ci} u_i\right) = g,\tag{1b}$$

$$\frac{\mathrm{d}}{\mathrm{d}z}\left(\rho_{ce} u_{ce}\right) = -g,\tag{1c}$$

where ϕ is the cell volume fraction, ρ_{ci} and ρ_{ce} are the superficial intracellular and extracellular calcium concentrations respectively, u_i and u_{ce} are the physical velocities of the cells and extracellular calcium respectively, f is the rate of change of cell volume fraction due to fluid exchange between ECF and cells, and g is the rate of change of superficial intracellular calcium concentration due to calcium exchange between ECF and cells. Functions f and g are positive when fluid and calcium respectively are being transferred from ECF to cells, and negative when fluid and calcium respectively are being transferred from cells to ECF. We next use equations (1a)-(1c), together with defined boundary conditions, to derive equations for calculating: keratinocyte velocity profiles $u_i(z)$ and transit times through the epidermis, the intracellular calcium profile $\rho_{ci}(z)$ and pattern of calcium exchange between keratinocytes and the ECF $g(z)$, and the dependence of the extracellular calcium profile $\rho_{ce}(z)$ on the permeability of the TJ barrier to calcium ions.

Model domain and boundary conditions

In this section, we define the model domain and provide two boundary conditions each for $u_i(z)$, $\rho_{ci}(z)$ and $\rho_{ce}(z)$ as part of our proposed theory, although not all of these conditions will be necessary for our subsequent analysis. The epidermal sublayers shown in Figure 2 are defined as follows: the SB in $0 \leq z \leq z_1$, the SS in $z_1 < z \leq z_2$, the SG in $z_2 < z \leq z_3$, the lower SC in $z_3 < z \leq z_4$ and the upper SC in $z_4 < z \leq z_5$. We assume that the two progenitor theory holds for human and murine epidermis [8]. In the two progenitor theory, the SB consists of stem cell and TA cell subpopulations which are suggested to form two spatially separate compartments [57, 58]. Hence we subdivide the SB into compartments consisting of stem cells, $0 \leq z \leq \theta z_1$, and TA cells, $\theta z_1 < z \leq z_1$, where θ is the volume fraction of the SB occupied by stem cells.

In our model, equation (1a) defines the dynamics of epidermal cells, whilst equations (1b) and (1c) define the dynamics of epidermal calcium. Because keratinocytes occupy all sublayers of the epidermis, the model domain for equation (1a) is $0 \leq z \leq z_5$. Keratinocytes cannot pass through the BM ($z = 0$)

but are continuously expelled at the skin surface ($z = z_5$), sloughed away during everyday activity [4]. Hence the boundary conditions for equation (1a) are

$$u_i(0) = 0, \tag{2a}$$

$$u_i(z_5) > 0. \tag{2b}$$

Our description of epidermal calcium profile formation treats the lower SC as a progressive barrier and the upper SC as an impermeable barrier to fluid and ion flow, based on TEWL experiments [15–17] and the observation of non-negligible calcium levels in the lower SC [33]. In our model we simplify this to treat the boundary between the lower and upper SC, denoted z_4, as the impermeable barrier to transport of fluid and ions. Hence the model domain for equations (1b) and (1c) is $0 \leq z \leq z_4$.

Intracellular calcium cannot travel across the BM because it is contained within keratinocytes, and is completely absent in the corneocytes of the upper SC [34, 37]. Hence the boundary conditions for equation (1b) are

$$\rho_{ci}(0)u_i(0) = 0, \tag{2c}$$

$$\rho_{ci}(z_4) = 0. \tag{2d}$$

The calcium present in the epidermis originates from movement of fluids and calcium across the BM [59], which at steady state must therefore act as a source of extracellular calcium with constant and positive concentration. Extracellular calcium is prevented from entering the upper SC by the impermeable barrier acting at z_4. Hence the boundary conditions for equation (1c) are

$$\rho_{ce}(0) = 0, \tag{2e}$$

$$\rho_{ce}(z_4)u_{ce}(z_4) = 0. \tag{2f}$$

For the analysis performed in this paper, we will only explicitly require two of the six boundary conditions listed here, equations (2a) and (2f).

Calculating keratinocyte velocity profiles and transit times

Using equation (1a), the keratinocyte velocity profile $u_i(z)$ is estimated from profiles that we now define for the cell volume fraction, $\phi(z)$, and volume exchange between cells and ECF, $f(z)$. We specify $f(z)$ as

$$f(z) = \begin{cases} s_0\phi, & 0 \leq z \leq \theta z_1, \\ s_1\phi, & \theta z_1 < z \leq z_1, \\ s_2\phi, & z_1 < z \leq z_2, \\ -s_3\phi, & z_2 < z \leq z_3, \\ 0, & z_3 < z \leq z_5. \end{cases} \tag{3}$$

This form expresses the different proliferation rates s_0 and s_1 of stem and TA cells in the SB [60], the rate of volume increase s_2 for keratinocytes migrating through the SS [11], the rate of volume decrease s_3 for keratinocytes migrating through the SG [12], and the relative structural inertness of corneocytes in the SC [61].

The cell volume fraction ϕ is assumed to be constant and equal to ϕ_v throughout both the viable sublayers (SB, SS and SG) and the lower SC [62]. The "bricks and mortar" architecture of the upper SC [14] constitutes a slow-moving relatively impenetrable barrier to fluid transport [63], equivalent to a sublayer consisting solely of keratinocyte-derived contents ($\phi = 1$). Hence the cell volume fraction profile $\phi(z)$ is specified as

$$\phi(z) = \begin{cases} \phi_v, & 0 \leq z \leq z_4, \\ 1, & z_4 < z \leq z_5. \end{cases} \tag{4}$$

The superficial keratinocyte velocity ϕu_i is assumed to be continuous at each of the sublayer boundaries, to ensure that cell mass flow is continuous throughout the epidermis. This consideration, together with equations (1a), (2a), (3) and (4), yield the keratinocyte velocity profile $u_i(z)$ as

$$
u_i(z) = \begin{cases}
s_0 z, & 0 \leq z \leq \theta z_1, \\
u_i(\theta z_1) + s_1(z - \theta z_1), & \theta z_1 \leq z \leq z_1, \\
u_i(z_1) + s_2(z - z_1), & z_1 \leq z \leq z_2, \\
u_i(z_2) - s_3(z - z_2), & z_2 \leq z \leq z_3, \\
u_i(z_3), & z_3 \leq z \leq z_4, \\
\phi_v u_i(z_4), & z_4 < z \leq z_5.
\end{cases}
\tag{5}
$$

Rates s_2 and s_3 are obtained from empirical observations of the ratio of keratinocyte volumes between the upper and lower boundaries of the SS, $V_1 > 1$ (net volume increase from lower to upper boundary), and the SG, $V_2 < 1$ (net volume decrease from lower to upper boundary), respectively, by use of the equations

$$
s_2 = \frac{u_i(z_1)}{z_2 - z_1}(V_1 - 1),
\tag{6a}
$$

$$
s_3 = \frac{u_i(z_2)}{z_3 - z_2}(1 - V_2).
\tag{6b}
$$

Equations (6a) and (6b) can be obtained using mathematical procedures similar to the derivation of $s_2(R)$ provided in Appendix B of [23].

Using the cell velocity profiles $u_i(z)$ defined by equations (5), (6a) and (6b), transit times through the various epidermal sublayers are calculated via

$$
\tau(z_a, z_b) = \int_{z_a}^{z_b} \frac{\mathrm{d}z}{u_i(z)},
\tag{7}
$$

where $\tau(z_a, z_b)$ is the average time taken for a keratinocyte to move from height above the BM z_a to height z_b. We assume that the transit through the SB can be approximated by the transit through the TA cell compartment, because the volume of SB occupied by stem cells is negligible compared to TA cells [64], and stem cells possess theoretically infinite transit time because they may never leave the SB. Hence, from equations (5) and (7) the epidermal transit times are given by

$$
\tau_{\mathrm{SB}} \approx \tau(z_0, z_1) = \frac{1}{s_1} \ln\left(\frac{u_i(z_1)}{u_i(z_0)}\right),
\tag{8a}
$$

$$
\tau_{\mathrm{SS}} = \tau(z_1, z_2) = \frac{1}{s_2} \ln(V_1),
\tag{8b}
$$

$$
\tau_{\mathrm{SG}} = \tau(z_2, z_3) = -\frac{1}{s_3} \ln(V_2),
\tag{8c}
$$

$$
\tau_{\mathrm{SC}} = \tau(z_3, z_5) = \frac{1}{u_i(z_3)}\left(z_4 - z_3 + \frac{z_5 - z_4}{\phi_v}\right).
\tag{8d}
$$

Calculating profiles of intracellular calcium and calcium exchange

In this section we show how the intracellular calcium profile $\rho_{ci}(z)$ and calcium exchange between keratinocytes and ECF $g(z)$, can be estimated from the total epidermal calcium profile $\rho(z)$.

The total calcium profile is a summation of intracellular and extracellular calcium profiles,

$$
\rho(z) = \rho_{ci}(z) + \rho_{ce}(z),
\tag{9}
$$

but extracellular calcium provides only a small contribution (2-10 mg/kg) to the total calcium profile in the epidermis (100-1100 mg/kg) [23, 36]. Hence, to estimate the intracellular calcium profile $\rho_{ci}(z)$ from the total calcium profile $\rho(z)$ using equation (9), at the scale of $\rho(z)$ we approximate the extracellular calcium distribution by a constant equal to its mean value throughout the epidermis,

$$\rho_{ce}(z) \approx r\rho_{ce}(0). \tag{10}$$

Here, r is a nondimensional factor equal to the ratio of the mean extracellular calcium concentration of all sublayers enclosed by $[0, z_4]$ to its concentration at the BM, and whose uncertainty bounds express the variation of the extracellular calcium concentration throughout these sublayers. The BM levels of total and extracellular calcium are related by

$$\rho(0) = \frac{\rho_{ce}(0)}{1 - \phi_v}, \tag{11}$$

an equation that was derived in Appendix C of [23] under two assumptions: (1) the motion of calcium across the BM only involves transfer between the free dermal and extracellular epidermal calcium, and (2) the BM provides no barrier for this transfer.

Combining equations (9)-(11), the intracellular calcium profile can be estimated from the total calcium profile via

$$\rho_{ci}(z) \approx \rho(z) - r(1 - \phi_v)\rho(0). \tag{12}$$

Equations (5) and (12) can be used to estimate the keratinocyte velocity profile $u_i(z)$ and intracellular calcium profile $\rho_{ci}(z)$. The pattern of calcium exchange $g(z)$ between cells and ECF can then be calculated from these two profiles using equation (1b) [23],

$$g(z) = \frac{\mathrm{d}}{\mathrm{d}z}(\rho_{ci}(z)u_i(z)).$$

In the following, we derive equations that link the extracellular calcium distribution to the permeability of the TJ barrier.

The effect of tight junctions on extracellular calcium diffusion

TJs regulate the extracellular flow of calcium ions in the SG [44, 45], and we model this as a reduction in the rate of extracellular calcium diffusion there. This effect is introduced through the term representing extracellular calcium flux, $\rho_{ce}u_{ce}$, that appears in equation (1c). The extracellular calcium flux $\rho_{ce}u_{ce}$ may consist of contributions from both diffusion and advection, the latter of which we expect to be negligible in epidermal sublayers where TJs are not present [23]. However, in epidermal sublayers where TJs are present, for advection to be negligible compared to diffusion we must ensure explicitly that the Péclet number, Pe, satisfies

$$\mathrm{Pe} = \frac{\hat{z}|u_e|}{D} \ll 1, \tag{13}$$

where $\hat{z} \leq z_4$ is the characteristic length scale over which the effects of diffusion and advection are being compared, $|u_e|$ is the ECF velocity that characterises the advective contribution, and D is the Fickian diffusion coefficient that characterises the diffusive contribution. In this paper we limit our analysis to cases for which inequality (13) is satisfied. We specify the extracellular calcium diffusion coefficient as

$$D(z) = \begin{cases} D_{\mathrm{Ca}}, & 0 \leq z \leq z_2, \\ \varepsilon_{\mathrm{Ca}}D_{\mathrm{Ca}}, & z_2 < z \leq z_3, \\ D_{\mathrm{Ca}}, & z_3 < z \leq z_4, \end{cases} \tag{14}$$

where D_{Ca} is the physical diffusion coefficient of calcium in the ECF in the absence of TJs, and ε_{Ca} represents the factor reduction in diffusion coefficient D_{Ca} induced by the presence of TJs.

In equation (14) we have assumed that TJs are evenly spread throughout the SG, which represents a simplification to the dynamic model we proposed for skin equivalent construct growth [46, 65], and that they are mostly absent in other sublayers. Whilst structures similar to the disassembly of TJs have been observed at the SG-SC interface [66] and TJ-like structures have been observed in the SC [67], for simplicity we assume that these structures provide no restriction on extracellular calcium ion flow there.

The permeability of a barrier can be written as a ratio of the diffusion coefficient of the substance within the barrier to the barrier's width [68]. Hence the permeability of the TJ barrier to calcium, P_{Ca}, which spans the SG z_2 to z_3, and has local diffusion coefficient there of $\varepsilon_{Ca}D_{Ca}$ according to equation (14), is

$$P_{Ca} = \frac{\varepsilon_{Ca}D_{Ca}}{z_3 - z_2}. \tag{15}$$

Combining equations (13)-(15), we find that the inequality

$$P_{Ca} \gg |u_e|, \tag{16}$$

is identical to the requirement given by inequality (13). Inequality (16) demonstrates that the permeability of the TJ barrier must be significantly larger than the local ECF velocity in order to disregard the contribution of advection to extracellular calcium dynamics. From [23] we expect that $\max\{|u_e|\}$ is $\mathcal{O}(1\,\text{nm}\,\text{s}^{-1})$ in the absence of TJs and aquaporins and hence we require

$$P_{Ca} \gg \mathcal{O}(1\,\text{nm}\,\text{s}^{-1}), \tag{17}$$

which effectively places a lower limit on the possible values of P_{Ca} that we investigate here. In summary, we include the effect of tight junctions on extracellular calcium dynamics in our model by assuming that the extracellular calcium flux $\rho_{ce}u_{ce}$ in equation (1c) is dominated by Fickian diffusion with coefficient D defined by equation (14), and this approach is valid if the permeability of the TJ barrier in the SG satisfies inequality (17).

Calculating the extracellular calcium profile

To derive an expression for the extracellular calcium profile $\rho_{ce}(z)$, we first equate (1b) and (1c) through the common term g, and assume that Fickian diffusion is the dominant contribution to the extracellular calcium flux, $\rho_{ce}u_{ce} = -D\,d\rho_{ce}/dz$, to obtain

$$\frac{d}{dz}(\rho_{ci}u_i) = \frac{d}{dz}\left(D\frac{d\rho_{ce}}{dz}\right). \tag{18}$$

Both sides of equation (18) are then integrated with limits z and z_4. We thereafter substitute boundary condition (2f), which yields

$$\frac{d\rho_{ce}}{dz}(z) = \frac{1}{D(z)}\left(\rho_{ci}(z)u_i(z) - \rho_{ci}(z_4)u_i(z_4)\right). \tag{19}$$

In epidermal sublayers where TJs are not present (i.e. everywhere except the SG), extracellular calcium kinetics are sufficiently dominated by diffusion that ρ_{ce} is constant [23]. Hence, replacing z by z' in equation (19), integrating this equation with limits 0 and z, and substituting equations (14) and (15),

yields

$$\rho_{ce}(z) = \begin{cases} \rho_{ce}(0), & 0 \leq z \leq z_2, \\[2ex] \rho_{ce}(0) + \int_{z_2}^{z} \dfrac{\rho_{ci}(z')u_i(z') - \rho_{ci}(z_4)u_i(z_4)}{(z_3 - z_2)P_{\mathrm{Ca}}} \mathrm{d}z', & z_2 \leq z \leq z_3, \\[2ex] \rho_{ce}(z_3), & z_3 < z \leq z_4. \end{cases} \tag{20}$$

In this equation, $\rho_{ci}(z)$ can be calculated from $\rho(z)$ using equation (12). Hence, equation (20) expresses the extracellular calcium profile $\rho_{ce}(z)$ in terms of $\rho(z)$, $u_i(z)$ and P_{Ca}, if inequality (17) is satisfied.

Relationship between tight junctions and the extracellular calcium profile

Finally, to clearly demonstrate the effect of the TJ barrier on the extracellular calcium profile, we define R_{ce} as the rise in extracellular calcium through the SG,

$$R_{ce} = \frac{\rho_{ce}(z_3)}{\rho_{ce}(z_2)}. \tag{21}$$

From equations (20) and (21), the relationship between the rise in extracellular calcium concentration through the TJ barrier in the SG, R_{ce}, and the permeability of this barrier, P_{Ca}, can be written in the elegant form

$$R_{ce} = 1 + \frac{P_0}{P_{\mathrm{Ca}}}, \tag{22}$$

where P_0 is a constant that depends on the epidermal keratinocyte velocity and calcium profiles,

$$P_0 = \frac{1}{(z_3 - z_2)\rho_{ce}(0)} \int_{z_2}^{z_3} (\rho_{ci}(z)u_i(z) - \rho_{ci}(z_4)u_i(z_4))\mathrm{d}z. \tag{23}$$

Using equations (22) and (23), the effects of a range of values for the permeability of the TJ barrier to calcium P_{Ca} on the defining feature of the extracellular calcium profile (its rise through the SG, R_{ce}) can be easily investigated, once the value of P_0 is known.

Results

The key predictions of our model are presented here. All mathematical equations were stated and derived in Materials and Methods. All parameters were obtained from experimental literature (see Text S1) and are stated in Table 1. In our calculations we also used the total calcium profiles $\rho(z)$ for human and murine epidermis reported in [28] and [26] respectively. All uncertainty bounds were calculated using error propagation formulae from [69, 70] under the assumption that the error distributions of all parameters were independent (i.e. zero covariance).

Epidermal transit times and keratinocyte velocities

Using equations (5)-(8) of our model, transit times through individual sublayers of human and murine epidermis were calculated. Our model's predictions of transit times mostly compared favourably with the literature values, as shown in Figure 3, although it is difficult to quantitatively compare these values due to the large uncertainty present in the transit times both from the literature and predicted by our model. The uncertainty in our model predictions of transit time is due to the uncertainty present in model parameters (Table 1), all of which were obtained from the experimental literature. Hence, a

better quantitative comparison of transit times from the literature and model requires experimental data possessing reduced uncertainty. We could not find literature values of transit time through murine SB so did not include comparisons for these.

The model prediction of transit time through human SC was much smaller than two of the three corresponding literature estimates. We attributed this discrepancy to our parameter estimate for human $V_2 = 0.54\pm0.10$, which was much larger than the estimate for murine $V_2 = 0.068\pm0.034$, the latter of which led to reasonable predictions of murine transit times. Hence, we modified our estimate of human V_2 to 0.100 ± 0.026, a value which was calculated from division of literature values for murine $V_1 \times V_2$ by human V_1 (see Text S1). The resulting predicted transit time for human SC agreed far better with the literature values for this transit time (Figure 3a). Because this modification of V_2 created agreement between estimates of keratinocyte volume size changes and transit times through our model, our analysis suggests that keratinocytes lose at least 87% of their volume during their disintegration in the SG, in both human and murine epidermis.

Keratinocyte velocity profiles $u_i(z)$ calculated using equations (5), (6a) and (6b) are shown in Figure 4. For the calculation of the human $u_i(z)$ profile, the modified V_2 was used. Regardless of the value of human V_2, in our model results there was little difference between the keratinocyte velocity distributions in the lower sublayers of human and murine epidermis. This conclusion extends to the upper sublayers if the keratinocyte volume decrease through human SG agrees with our modified value for V_2 (i.e. $90.0\pm2.6\%$ volume reduction).

The extracellular calcium rise mediated by tight junctions

Figures 5a and 5b show the relationships between the rise in extracellular calcium through the SG and the permeability of the TJ barrier there, for human and murine epidermis respectively, that were predicted by our model using equations (22) and (23). Results are only shown for $P_{Ca} \geq 5\,\mathrm{nm\,s}^{-1}$ in order to satisfy applicability condition (17). As indicated by equation (22), each of these plots is characterised by one parameter P_0 which depends on the epidermal keratinocyte velocity and calcium profiles; to construct Figures 5a and 5b we obtained $P_0 = 3.8\pm3.2\,\mathrm{nm\,s}^{-1}$ and $P_0 = 10\pm8\,\mathrm{nm\,s}^{-1}$ for human and murine epidermis respectively. From these values, we calculated the permeability of the TJ barrier by assuming that the extracellular calcium concentration rises by at least 50% across the SG (i.e. $R_{ce} = 1.5$), based on experimental data for extracellular calcium distributions (see Table S1). This calculation yielded TJ barrier permeabilities to calcium ions of $P_{Ca} < 15\,\mathrm{nm\,s}^{-1}$ for human epidermis and $P_{Ca} < 37\,\mathrm{nm\,s}^{-1}$ for murine epidermis.

Extracellular and intracellular calcium profiles

Extracellular and intracellular epidermal calcium profiles, predicted from total calcium profiles $\rho(z)$ and keratinocyte velocity profiles $u_i(z)$ using the equations of our model, are shown in Figures 6a and 6b for human and murine epidermis respectively. The intracellular calcium profiles $\rho_{ci}(z)$ were nearly identical to the experimental total calcium profiles [26, 28] from which they were calculated. The extracellular calcium profiles $\rho_{ce}(z)$, calculated using equation (20), possessed constant concentration in the SB and SS due to rapid diffusion of this calcium throughout the ECF, and a rise through the SG due to the presence of TJs (see Figure 2). In Figures 6a and 6b we chose the permeability of the TJ barrier to calcium as $P_{Ca} = 8\,\mathrm{nm\,s}^{-1}$ and $P_{Ca} = 20\,\mathrm{nm\,s}^{-1}$ for human and murine epidermis respectively, as these values yielded a calcium rise through the SG of $R_{ce} \approx 1.5$ in qualitative agreement with the experimental data (Table S1). These values of TJ permeability barrier ($8\,\mathrm{nm\,s}^{-1}$ for human epidermis and $20\,\mathrm{nm\,s}^{-1}$ for murine epidermis) also clearly satisfy the previously stated inequalities of $P_{Ca} < 15\,\mathrm{nm\,s}^{-1}$ for human epidermis and $P_{Ca} < 37\,\mathrm{nm\,s}^{-1}$ for murine epidermis.

Patterns of calcium exchange $g(z)$ between keratinocytes and the ECF, predicted using equation (1b), are shown in Figures 7a and 7b for human and murine epidermis respectively. In both plots, a distinct

switch in calcium exchange from cellular influx (positive) to outflux (negative) was predicted at the SS-SG boundary, in agreement with our theory (Figure 2).

Discussion

In this paper we investigated the hypothesis that the intracellular and extracellular epidermal calcium profiles in unwounded skin are attributed to three key mechanisms: (1) the primary SC barrier which selectively allows water but not calcium to leave the epidermis [35], (2) progressive intracellular calcium accumulation through the lower epidermal sublayers [36] followed by a phenotypic switch at the SS-SG boundary to expulsion of intracellular calcium to the ECF above this boundary [23], and (3) reduced diffusion of extracellular calcium ions in the SG due to the secondary TJ barrier [43] which together with the aforementioned expulsion of calcium from intracellular stores causes the extracellular calcium concentration to become elevated towards the skin surface [44, 46]. This hypothesis was formulated in a mathematical model (described in Materials and Methods) that predicts intracellular and extracellular calcium profiles in human and murine epidermis (Figure 6) which agree well with semi-quantitative experimental data available for these profiles [32–34].

We first parameterised the keratinocyte velocity profiles in human and murine epidermis, which is a requirement for the proper investigation of intracellular calcium dynamics. The calculation of these velocity profiles improves over our previous model [23] by including consideration of the slower cycling stem cell subpopulation of the SB [60] and the keratinocyte volume changes through the SS [11], and validating the velocity profiles against several sources of experimental data for keratinocyte transit times in the SB (human only) and the three suprabasal sublayers (SS, SG and SC).

The presence of stem cells in interfollicular epidermis is currently a hotly debated topic [6, 8]. Stem cells have little effect on the keratinocyte velocity profiles and subsequent calculations due to their small potential occupancy of the SB (1-10%, [64]), but their inclusion in the present model is advantageous as it allows validation of these profiles against transit times in the SB. Although our model assumed that the traditional two progenitor theory holds, it can be reduced to the single progenitor theory by setting $\theta = 0$, in which case s_1 is the proliferation rate of these progenitors.

The validation of keratinocyte velocity profiles against epidermal transit time data (Figure 3) was made somewhat difficult by the uncertainty in both our predicted velocity profiles and the data. Despite this, the validation clearly supported the modification of one of our parameters, the volume change in keratinocytes through the SG for human epidermis (V_2), from its value used in our previous model of unwounded epidermis ($R = 1 - V_2$, [23]). Our results suggested that keratinocytes in human epidermis may reduce their volume by approximately 10-fold during terminal differentiation and that this reduction may be even larger in murine epidermis.

We next investigated the effect of the permeability of the TJ barrier to calcium ions, P_{Ca}, on the extracellular calcium distribution. Our model predictions of P_{Ca} carry large uncertainty due to the cumulative uncertainty in all parameters used to calculate them, and are only applicable if P_{Ca} is significantly greater than $\mathcal{O}(1\,\text{nm s}^{-1})$. Despite these limitations, we found that a value of P_{Ca} that is less than $15\,\text{nm s}^{-1}$ for human epidermis and less than $37\,\text{nm s}^{-1}$ for murine epidermis is sufficient to cause the extracellular calcium distribution to rise by at least 50% across the SG, which is a typical pattern seen in the experimental semi-quantitative calcium profiles measured using ion capture cytochemistry [32–34]. Kirschner *et al.* [45] recently reported that the permeability of the TJ barrier to calcium ions in cultured primary human keratinocytes was 40-80 nm s^{-1} within 1-4 days after a switch to high calcium medium (this switch is the key step in triggering keratinocytes to stratify *in vitro* [2]). These larger experimentally-found values of P_{Ca}, which indicate a reduced TJ barrier to calcium ions, may be attributable to the impaired barrier formation demonstrated by cultured keratinocytes compared to native skin [33].

To further elucidate this point, the transepithelial resistance (TER) of the TJ barrier in the submerged human keratinocytes reported by Kirschner *et al.* [45] reached a steady-state value of $\sim$150 $\Omega\,\text{cm}^2$ after

4 days. In contrast, Sun *et al.* [71] and Petrova *et al.* [72] reported that the TER of the TJ barrier in human epidermal equivalents grown at an air-liquid interface (which yields a better representation of native epidermis than submerged keratinocytes [73]) rose to over $1000\,\Omega\,\mathrm{cm}^2$ prior to formation of the lipid barrier. TER is the most common experimental measure of TJ barrier permeability [74], and is inversely related to it [75]. These considerations together suggest that the permeability of the TJ barrier should be less in native epidermis than in submerged keratinocytes grown *in vitro*. This agrees with our model prediction of a TJ barrier permeability to calcium ions in human epidermis that is less than the TJ barrier permeability to calcium ions experimentally observed in cultured human keratinocytes [45].

Finally, we calculated profiles of intracellular calcium, extracellular calcium and the exchange between these two (Figures 6 and 7), from experimentally-reported total calcium profiles for human epidermis [28] and murine epidermis [26]. For the calculation of extracellular calcium profiles, we set the value of the calcium permeability of the epidermal TJ barrier so that it approximates an extracellular calcium concentration rise of 50% through the SG. The resulting profiles (Figure 6) indicate that the physical intracellular calcium concentration is typically greater than the physical extracellular calcium concentration. Bearing in mind that intracellular and extracellular calcium are present in cells and ECF which occupy $\geq 93\%$ and $\leq 7\%$ of the epidermal volume respectively [36, 40], our model clearly predicts that intracellular calcium is the main source of the epidermal calcium profile [23].

The predicted pattern of calcium exchange between keratinocytes and the ECF (Figures 6a and 6b) is significantly modified from our previous calculations of this pattern (Figures 4c and 4d in [23]), due to the improved parameterisations used here for the keratinocyte volume changes through the SS and the SG, the former of which was assumed to be negligible in our previous models [23, 46]. The updated predictions cast doubt over the assertions in [23] that calcium influx is constant in the SB and SS and that there is a calcium influx peak in the lower SG potentially due to loss of plasma membrane Ca^{2+}-ATPase [76]. However, the improved parameterisations confirmed the key finding of [23] that a change in calcium exchange from cellular influx to outflux actively regulates the epidermal calcium profile. The present theoretical work provides stronger evidence that this active regulation is caused by a phenotypic switch located at the SS-SG boundary (Figure 7). The origin of this distinct switch in calcium exchange is currently being investigated with time-dependent continuum models developed by members of our research group [77].

Whilst our quantitative theory is able to predict the key features of intracellular and extracellular calcium profiles in unwounded epidermis, it has some potential weaknesses. We have assumed that the SC and TJ barriers are inert entities which regulate the epidermal calcium profile without any existing feedback processes, which is reasonable for considering unwounded epidermis as it represents a steady state condition. However, the formation of these barriers is likely to be dependent both on each other [78] and on the presence of the local calcium concentration [79, 80]. Hence this model cannot be immediately extended to consider temporal dynamics of wounded skin without specifying additional assumptions about the effects of epidermal calcium on the TJ and SC barriers. This is especially important since the rapid secretion by keratinocytes of lamellar bodies (the precursor to lipids that form the "mortar" component of the SC barrier) following barrier disruption is primarily controlled by calcium ions in the SG [13]. Whilst our conceptual model provides a feasible explanation for the formation of the calcium profile, especially as model parameters were obtained from experimental data, we cannot rule out the possibility of the contribution to this profile from other factors, such as the lipid barrier [78], electrophoresis [81], or binding of calcium to molecules such as profilaggrin [82]. In addition, if the factors that contribute substantially to the epidermal calcium profile occur on length scales of cells or smaller, our mathematical treatment of the epidermis as a porous medium may not be appropriate, and individual cell-based models (e.g. [83,84]) are more suitable.

Our estimates of the TJ barrier permeability to calcium may require revision if the width of this barrier is larger or smaller than the SG. The effective TJ barrier may be larger than the SG if the TJ-like structures observed in the SC [67] reduce the extracellular calcium diffusion rate sufficiently there to yield

protrusion of the extracellular calcium rise into the lower SC. On the other hand, the width of the TJ barrier may be smaller than the thickness of the SG, as recent experiments in mouse ear epidermis have suggested that only the TJs forming apically between the second of three cell monolayers of the SG are primarily responsible for its barrier [85]. Future experimental work may resolve this question about the localisation of TJ barrier function.

The investigations of the TJ barrier with our model were also limited to values for its permeability to calcium that satisfy inequality (17), which mathematically states the assumption that the TJ barrier permeability is significantly larger than the local ECF velocity in the absence of TJs. ECF flow is likely to be important for maintaining healthy unwounded epidermis, as occlusion of wounded skin by a vapour-permeable dressing (which permits low rates of transcutaneous water movement) is an adequate substitute for the SC whilst a vapour-impermeable dressing is not [35]. Future direct measurements of the TJ barrier permeability to calcium ions in native epidermis will hopefully confirm the applicability of inequality (17) and our subsequent mathematical theory relating the TJ barrier permeability to the extracellular calcium profile.

In conclusion, we have proposed and mathematically investigated a theory of calcium profile formation in unwounded mammalian epidermis governed by: the impermeable barrier of the SC, TJ-limited calcium diffusion in the SG, and a phenotypic switch in calcium exchange between keratinocytes and ECF at the SS-SG boundary. Future experimental results gained from improved measurement techniques [39,86] may refine the presented theory and reduce the uncertainty in our model predictions. There are many possibilities for future theoretical work, including the investigation of temporally changing epidermal states for which calcium plays a major role (e.g. wound healing [35], psoriasis [34], and stratification of keratinocyte cultures [2]), and the consideration of our proposed calcium kinetics in individual cell-based models of epidermal homeostasis [83]. We intend that this paper provides a conceptual and quantitative model for future experimental and theoretical research to examine, modify and update, as our understanding of epidermal calcium profile formation becomes increasingly advanced.

Acknowledgments

References

1. Menon G, Elias P, Lee S, Feingold K (1992) Localization of calcium in murine epidermis following disruption and repair of the permeability barrier. Cell Tissue Res 270: 503-512.

2. Hennings H, Michael D, Cheng C, Steinert P, Holbrook K, et al. (1980) Calcium regulation of growth and differentiation of mouse epidermal cells in culture. Cell 19: 245-254.

3. Houben E, Paepe KD, Rogiers V (2007) A keratinocyte's course of life. Skin Pharmacol Physiol 20: 122-132.

4. Elias P, Feingold K, editors (2006) Skin barrier. Taylor and Francis, New York.

5. Simons BD, Clevers H (2011) Strategies for homeostatic stem cell self-renewal in adult tissues. Cell 145: 851-862.

6. Clayton E, Doupé DP, Klein AM, Winton DJ, Simons BD, et al. (2007) A single type of progenitor cell maintains normal epidermis. Nature 446: 185-189.

7. Doupé DP, Klein AM, Simons BD, Jones PH (2010) The ordered architecture of murine ear epidermis is maintained by progenitor cells with random fate. Dev Cell 18: 317-323.

8. Mascré G, Dekoninck S, Drogat B, Youssef KK, Broh'ee S, et al. (2012) Distinct contribution of stem and progenitor cells to epidermal maintenance. Nature 489: 257-262.

9. Watt F (2001) Stem cell fate and patterning in mammalian epidermis. Curr Opin Genet Dev 11: 410-417.

10. Fuchs E (2008) Skin stem cells: rising to the surface. J Cell Biol 180: 273-284.

11. Corcuff P, Bertrand C, Leveque J (1993) Morphometry of human epidermis *in vivo* by real-time confocal microscopy. Arch Dermatol Res 285: 475-481.

12. Norlén L, Al-Amoudi A (2004) Stratum corneum keratin structure, function, and formation: the cubic rod-packing and membrane templating model. J Invest Dermatol 123: 715-732.

13. Feingold K (2007) The role of epidermal lipids in cutaneous permeability barrier homeostasis. J Lipid Res 48: 2531-2546.

14. Nemes Z, Steinert PM (1999) Bricks and mortar of the epidermal barrier. Exp Mol Med 31: 5-19.

15. Kalia YN, Alberti I, Sekkat N, Curdy C, Naik A, et al. (2000) Normalization of stratum corneum barrier function and transepidermal water loss *in vivo*. Pharm Res 17: 1148-1150.

16. Bashir SJ, Chew AL, Anigbogu A, Dreher F, Maibach HI (2001) Physical and physiological effects of stratum corneum tape stripping. Skin Res Technol 7: 40-48.

17. Yow HN, Wu X, Routh AF, Guy RH (2009) Dye diffusion from microcapsules with different shell thickness into mammalian skin. Eur J Pharm Biopharm 72: 62-68.

18. Pierard GE, Goffin V, Hermanns-Le T, Pierard-Franchimont C (2000) Corneocyte desquamation. Int J Mol Med 6: 217-238.

19. Berridge M, Bootman M, Roderick H (2003) Calcium signalling: dynamics, homeostasis and remodelling. Nat Rev Mol Cell Biol 4: 517-529.

20. Clapham D (2007) Calcium signaling. Cell 131: 1047-1058.

21. Meldolesi J, Grohovaz F (2001) Total calcium ultrastructure: advances in excitable cells. Cell Calcium 30: 1-8.

22. Brini M, Carafoli E (2009) Calcium pumps in health and disease. Physiol Rev 89: 1341-1378.

23. Adams MP, Mallet DG, Pettet GJ (2012) Active regulation of the epidermal calcium profile. J Theor Biol 301: 112-121.

24. Malmqvist KG, Carlsson LE, Forslind B, Roomans GM, Akselsson KR (1984) Proton and electron microprobe analysis of human skin. Nucl Instrum Meth B 3: 611-617.

25. Pallon J, Malmqvist KG, Werner-Linde Y, Forslind B (1996) PIXE analysis of pathological skin with special reference to psoriasis and atopic dry skin. Cell Mol Biol 42: 111-118.

26. Mauro T, Bench G, Sidderas-Haddad E, Feingold K, Elias P, et al. (1998) Acute barrier perturbation abolishes the Ca^{2+} and K^+ gradients in murine epidermis: quantitative measurement using PIXE. J Invest Dermatol 111: 1198-1201.

27. Elias PM, Nau P, Hanley K, Cullander C, Crumrine D, et al. (1998) Formation of the epidermal calcium gradient coincides with key milestones of barrier ontogenesis in the rodent. J Invest Dermatol 110: 399-404.

28. Behne M, Tu CL, Aronchik I, Epstein E, Bench G, et al. (2003) Human keratinocyte ATP2C1 localizes to the Golgi Ca^{2+} stores. J Invest Dermatol 121: 688-694.

29. Forslind B, Roomans G, Carlsson LE, Malmqvist K, Akselsson K (1984) Elemental analysis on freeze-dried sections of human skin: studies by electron microprobe and particle induced X-ray emission analysis. Scan Electron Microsc Pt 2: 755-759.

30. Borgers M, Thoné F, Nueten JMv (1981) The subcellular distribution of calcium and the effects of calcium-antagonists as evaluated with a combined oxalate-pyroantimonate technique. Acta Histochem Suppl 24: S327-S332.

31. Reempts Jv, Borgers M, Offner F (1982) Ultrastructural localization of calcium in the rat retina with a combined oxalate-pyroantimonate technique. Histochem J 14: 517-522.

32. Menon G, Grayson S, Elias P (1985) Ionic calcium reservoirs in mammalian epidermis: Ultrastructural localization by ion-capture cytochemistry. J Invest Dermatol 84: 508-512.

33. Vičanová J, Boelsma E, Mommaas A, Kempenaar J, Forslind B, et al. (1998) Normalization of epidermal calcium distribution profile in reconstructed human epidermis is related to improvement of terminal differentiation and stratum corneum barrier formation. J Invest Dermatol 111: 97-106.

34. Menon G, Elias P (1991) Ultrastructural localization of calcium in psoriatic and normal human epidermis. Arch Dermatol 127: 57-63.

35. Elias P, Ahn S, Brown B, Crumrine D, Feingold K (2002) Origin of the epidermal calcium gradient: regulation by barrier status and role of active *vs* passive mechanisms. J Invest Dermatol 119: 1269-1274.

36. Celli A, Sanchez S, Behne M, Hazlett T, Gratton E, et al. (2010) The epidermal Ca^{2+} gradient: measurement using the phasor representation of fluorescent lifetime imaging. Biophys J 98: 911-921.

37. Ahn SK, Hwang SM, Jiang SJ, Choi EH, Lee SH (1999) The changes of epidermal calcium gradient and transitional cells after prolonged occlusion following tape stripping in the murine epidermis. J Invest Dermatol 113: 189-195.

38. Denda M, Hosoi J, Asida Y (2000) Visual imaging of ion distribution in human epidermis. Biochem Biophys Res Commun 272: 134-137.

39. Behne MJ, Sanchez S, Barry NP, Kirschner N, Meyer W, et al. (2011) Major translocation of calcium upon epidermal barrier insult: imaging and quantification via FLIM/Fourier vector analysis. Arch Dermatol Res 303: 103-115.

40. Elias P, Leventhal M (1979) Intercellular volume changes and cell surface expansion during cornification. Clin Res 27: 525A.

41. Halprin K, Ohkawara A (1967) Glucose entry into the human epidermis: II. The penetration of glucose into the human epidermis *in vitro*. J Invest Dermatol 49: 561-568.

42. Brandner JM, Kief S, Grund C, Rendl M, Houdek P, et al. (2002) Organization and formation of the tight junction system in human epidermis and cultured keratinocytes. Eur J Cell Biol 81: 253-263.

43. Kirschner N, Houdek P, Fromm M, Moll I, Brandner JM (2010) Tight junctions form a barrier in human epidermis. Eur J Cell Biol 89: 839-842.

44. Kurasawa M, Maeda T, Oba A, Yamamoto T, Sasaki H (2011) Tight junction regulates epidermal calcium ion gradient and differentiation. Biochem Biophys Res Commun 406: 506-511.

45. Kirschner N, Rosenthal R, Furuse M, Moll I, Fromm M, et al. (2013) Contribution of tight junction proteins to ion, macromolecule, and water barrier in keratinocytes. J Invest Dermatol 133: 1161-1169.

46. Adams MP, Mallet DG, Pettet GJ (2012) A continuum model of the growth of engineered epidermal skin substitutes. ANZIAM J (EMAC 2011) 53: C90-C109.

47. Lemon G, King JR, Byrne HM, Jensen OE, Shakesheff KM (2006) Mathematical modelling of engineered tissue growth using a multiphase porous flow mixture theory. Journal of Mathematical Biology 52: 571-594.

48. Please C, Pettet G, McElwain D (1998) A new approach to modelling the formation of necrotic regions in tumours. Appl Math Lett 11: 89-94.

49. Please C, Pettet G, McElwain D (1999) Avascular tumour dynamics and necrosis. Math Mod Meth Appl S 9: 569-579.

50. Landman K, Please C (2001) Tumour dynamics and necrosis: surface tension and stability. IMA J Math Appl Med 18: 131-158.

51. Lemon G, King J (2007) Multiphase modelling of cell behaviour on artificial scaffolds: effects of nutrient depletion and spatially nonuniform porosity. Math Med Biol 24: 57-83.

52. Kitson N, Thewalt JL (2000) Hypothesis: the epidermal permeability barrier is a porous medium. Acta Dermato-Venereologica Supp 208: 12-15.

53. Tsutsumi M, Inoue K, Denda S, Ikeyama K, Goto M, et al. (2009) Mechanical-stimulation-evoked calcium waves in proliferating and differentiated human keratinocytes. Cell Tissue Res 338: 99-106.

54. Furuse M, Hata M, Furuse K, Yoshida Y, Haratake A, et al. (2002) Claudin-based tight junctions are crucial for the mammalian epidermal barrier: a lesson from claudin-1-deficient mice. The Journal of Cell Biology 156: 1099-1111.

55. Ågren J, Zelenin S, Håkansson M, Elköf AC, Aperia A, et al. (2003) Transepidermal water loss in developing rats: role of aquaporins in the immature skin. Pediatric Research 53: 558-565.

56. Sougrat R, Morand M, Gondran C, Barré P, Gobin R, et al. (2002) Functional expression of AQP3 in human skin epidermis and reconstructed epidermis. The Journal of Investigative Dermatology 118: 678-685.

57. Jensen UB, Lowell S, Watt FM (1999) The spatial relationship between stem cells and their progeny in the basal layer of human epidermis: a new view based on whole-mount labelling and lineage analysis. Development 126: 2409-2418.

58. Ghazizadeh S, Taichman LB (2005) Organization of stem cells and their progeny in human epidermis. The Journal of Investigative Dermatology 124: 367-372.

59. Menon G, Elias P, Feingold K (1994) Integrity of the permeability barrier is crucial for maintenance of the epidermal calcium gradient. Br J Dermatol 130: 139-147.

60. Potten C, Booth C (2002) Keratinocyte stem cells: a commentary. J Invest Dermatol 119: 888-899.

61. Forslind B, Lindberg M, editors (2004) Skin, hair, and nails: structure and function. Marcel Dekker, New York.

62. Gandolfi A, Iannelli M, Marinoschi G (2011) An age-structured model of epidermis growth. J Math Biol 62: 111-141.

63. Blank I, III JM, Emslie A, Simon I, Apt C (1984) The diffusion of water across the stratum corneum as a function of its water content. J Invest Dermatol 82: 188-194.

64. Li A, Simmons P, Kaur P (1998) Identification and isolation of candidate human keratinocyte stem cells based on cell surface phenotype. P Natl Acad Sci USA 85: 3902-3907.

65. Adams MP, Mallet DG, Pettet GJ (2012) Solution methods for advection-diffusion-reaction equations on growing domains and subdomains, with application to modelling skin substitutes. Proceedings of the 4th International Conference on Computational Methods (ICCM2012), Gold Coast, Australia, Paper 230 .

66. Schlüter H, Wepf R, Moll I, Franke WW (2004) Sealing the live part of the skin: the integrated meshwork of desmosomes, tight junctions and curvilinear ridge structures in the cells of the uppermost granular layer of the human epidermis. European Journal of Cell Biology 83: 655-665.

67. Haftek M, Callejon S, Sandjeu Y, Padois K, Falson F, et al. (2011) Compartmentalization of the human *stratum corneum* by persistent tight junction-like structures. Experimental Dermatology 20: 617-621.

68. Potts RO, Guy RH (1992) Predicting skin permeability. Pharmaceutical Research 9: 663-669.

69. Mandel J (1964) The statistical analysis of experimental data. John Wiley & Sons, Inc.

70. Ku HH (1966) Notes on the use of propagation of error formulas. Journal of Research of the National Bureau of Standards Section C: Engineering and Instrumentation 70C: 263-273.

71. Sun R, Celli A, Crumrine D, Hupe M, Adame L, et al. (2014) Lowered humidity produces human epidermal equivalents with enhanced barrier properties. Tissue Eng Pt C-Meth Jun 16 [Epub ahead of print].

72. Petrova A, Celli A, Jacquet L, Dafou D, Crumrine D, et al. (2014) 3D in vitro model of a functional epidermal permeability barrier from human embryonic stem cells and induced pluripotent stem cells. Stem Cell Rep 2: 675-689.

73. Bernstam L, Vaughan F, Bernstein I (1986) Keratinocytes grown at the air-liquid interface. In Vitro Cellular and Developmental Biology 22: 695-705.

74. Günzel D, Krug S, Rosenthal R, Fromm M (2010) Biophysical methods to study tight junction permeability. Current Topics in Membranes 65: 39-78.

75. Madara J (1998) Regulation of the movement of solutes across tight junctions. Annual Review of Physiology 60: 143-159.

76. Cho JK, Bikle D (1997) Decrease of Ca^{2+}-ATPase activity in human keratinocytes during calcium-induced differentiation. J Cell Physiol 172: 146-154.

77. Personal communications with G. J. Pettet (2014).

78. Celli A, Zhai Y, Jiang Y, Crumrine D, Elias P, et al. (2012) Tight junction properties change during epidermis development. Experimental Dermatology 21: 783-801.

79. Bleich M, Shan Q, Himmerkus N (2012) Calcium regulation of tight junction permeability. Annals of the New York Academy of Sciences 1258: 93-99.

80. Baek JH, Lee SE, Choi KJ, Choi EH, Lee SH (2013) Acute modulations in stratum corneum permeability barrier function affect claudin expression and epidermal tight junction function via changes of epidermal calcium gradient. Yonsei Medical Journal 54: 523-528.

81. Cornelissen L, Oomens C, Huyghe J, Baaijens F (2007) Mechanisms that play a role in the maintenance of the calcium gradient in the epidermis. Skin Res Technol 13: 369-376.

82. Markova N, Marekov L, Chipev C, Gan S, Idler W, et al. (1993) Profilaggrin is a major epidermal calcium-binding protein. Mol Cell Biol 13: 613-625.

83. Grabe N, Neuber K (2005) A multicellular systems biology model predicts epidermal morphology, kinetics and Ca^{2+} flow. Bioinformatics 21: 3541-3547.

84. Sun T, Adra S, Smallwood R, Holcombe M, MacNeil S (2009) Exploring hypotheses of the actions of TGF-β1 in epidermal wound healing using a 3D computational multiscale model of the human epidermis. PLoS One 4: e8515.

85. Kubo A, Nagao K, Yokouchi M, Sasaki H, Amagai M (2009) External antigen uptake by langerhans cells with reorganization of epidermal tight junction barriers. The Journal of Experimental Medicine 206: 2937-2946.

86. Bloksgaard M, Brewer K, Bagatolli LA (2013) Structural and dynamical aspects of skin studied by multiphoton excitation fluorescence microscopy-based methods. European Journal of Pharmaceutical Sciences 50: 586-594.

87. Halprin K (1972) Epidermal "turnover time" - a re-examination. Br J Dermatol 86: 14-19.

88. Iizuka H (1994) Epidermal turnover time. J Dermatol Sci 8: 215-217.

89. Rothberg S, Crounse RG, Lee JL (1961) Glycine-C^{14} incorporation into the proteins of normal stratum corneum and the abnormal stratum corneum of psoriasis. J Invest Dermatol 37: 497-505.

90. Baker H, Kligman AM (1967) Technique for estimating turnover time of human stratum corneum. Archives of Dermatology 95: 408-411.

91. Epstein W, Maibach H (1965) Cell renewal in human epidermis. Arch Dermatol 92: 462-468.

92. Downes AM, Matoltsy AG, Sweeney TM (1967) Rate of turnover of the stratum corneum in hairless mice. J Invest Dermatol 49: 400-405.

93. Potten CS, Saffhill R, Maibach HI (1987) Measurement of the transit time for cells through the epidermis and stratum corneum of the mouse and guinea-pig. Cell Tissue Kinet 20: 461-472.

94. Potten C (1975) Epidermal transit times. Br J Dermatol 93: 649-658.

95. Personal communications with T. M. Mauro and A. Celli (2013).

96. Bergstresser PR, Pariser RJ, Taylor JR (1978) Counting and sizing of epidermal cells in normal human skin. J Invest Dermatol 70: 280-284.

97. Rowden G (1975) Ultrastructural studies of keratinized epithelia of the mouse. III. Determination of the volumes of nuclei and cytoplasm of cells in murine epidermis. J Invest Dermatol 64: 1-3.

98. Rodrigues LHT, Maia Campos PMBG (2002) Comparative study of the effects of cosmetic formulations with or without hydroxy acids on hairless mouse epidermis by histopathologic, morphometric, and stereologic evaluation. J Cosmet Sci 53: 269-282.

99. Allen T, Potten C (1976) Ultrastructural site variations in mouse epidermal organization. J Cell Sci 21: 341-359.

100. Castelijns F, Ezendam J, Latijnhouwers M, Vlijmen-Willems IV, Zeeuwen P, et al. (1998) Epidermal cell kinetics by combining *in situ* hybridization and immunohistochemistry. Histochem J 30: 869-877.

101. Potten C (1975) Epidermal cell production rates. J Invest Dermatol 65: 488-500.

102. Kampmeyer P (1952) The temperature dependence of viscosity for water and mercury. J Appl Phys 23: 99-102.

103. Li YH, Gregory S (1974) Diffusion of ions in sea water and in deep-sea sediments. Geochim Cosmochim Ac 38: 703-714.

104. Williams E, Heusch A, McCarthy P (2008) Thermal screening of facial skin arterial hot spots using non-contact infrared radiometry. Physiol Meas 29: 341-348.

Figure Legends

Figure 1. The epidermal calcium distribution. (a) Typical shape of the total profile found quantitatively using PIXE (for examples in the experimental literature, see [26, 28]). (b) Typical shape of the semi-quantitative intracellular ([Cai]) and extracellular ([Cae]) profiles measured using ion capture cytochemistry (for examples in the experimental literature, see [32–34]).

Figure 2. Proposed conceptual model of epidermal calcium profile formation in unwounded skin. The mathematical model presented in this paper simplifies the progressive barrier in the lower SC to a distinct barrier at the lower-upper SC boundary.

Figure 3. Comparison of epidermal sublayer transit times predicted by our model with experimental literature values. (a) Human literature values from [87–91]. (b) Murine literature values from [92–94]. *Model prediction in the SB was independent of the value of V_2. **Value may include some residence time in the SB.

Figure 4. Keratinocyte velocity profiles predicted by our model. For (a) the human keratinocyte velocity profile, the modified $V_2 = 0.100 \pm 0.026$ was used in its calculation. The solid and dashed lines represent the mean values and uncertainty bounds ($\pm$ SD) respectively.

Figure 5. Extracellular calcium rise through the SG vs TJ permeability to calcium predicted by our model. The solid and dashed lines represent the mean values and uncertainty bounds ($\pm$ SD) respectively.

Figure 6. Physical intracellular ([Cai]) and extracellular ([Cae]) epidermal calcium profiles predicted by our model. These profiles are calculated from experimental total calcium profiles reported in [26, 28]. [Cae] profiles are shown for TJ barriers that yield a calcium rise through the SG of $R_{ce} \approx 1.5$: (a) $P_{\text{Ca}} = 8\,\text{nm}\,\text{s}^{-1}$ for human epidermis and (b) $P_{\text{Ca}} = 20\,\text{nm}\,\text{s}^{-1}$ for murine epidermis.

Figure 7. Keratinocyte calcium influx profiles $g(z)$ in the epidermis predicted by our model. These profiles are calculated from experimental total calcium profiles reported in [26, 28].

Tables

Table 1. Model Parameters

| Parameter	Value and Reference	
	Human	**Murine**
Stem cell volume fraction of the SB, θ	0.055±0.045 [64]	0.055±0.045 [64]
Height of the SB-SS boundary above the BM, z_1	45 μm [95]	20 μm [26]
Height of the SS-SG boundary above the BM, z_2	75 μm [95]	60 μm [26]
Height of the SG-SC boundary above the BM, z_3	105 μm [95]	90 μm [26]
Height of the inner SC-outer SC boundary above the BM, z_4	118.5±1.5 μm [15, 16, 28]	94±2 μm [17, 26]
Thickness of the epidermis, z_5	125 μm [28]	100 μm [26]
Ratio of keratinocyte volumes SG:SB, V_1	1.9±0.5 [96]	2.8±1.4 [97, 98]
Ratio of keratinocyte volumes SC:SG, V_2	0.54±0.10 (original) [12] 0.100±0.026 (modified) [96, 99]	0.068±0.03 [97–99]
Proliferation rate of stem cells in the SB, s_0	$5.6\times10^{-7}\,\mathrm{s}^{-1}$ [60]	$1.4\times10^{-6}\,\mathrm{s}^{-1}$ [60]
Proliferation rate of TA cells in the SB, s_1	$(1.7\pm1.1)\times10^{-6}\,\mathrm{s}^{-1}$ [88, 100]	$(2.8\pm1.3)\times10^{-6}\,\mathrm{s}^{-1}$ [101]
Physical diffusion coefficient of calcium in the ECF, D_{Ca}	$1\times10^{-9}\,\mathrm{m}^2\,\mathrm{s}^{-1}$ [102–104]	$1\times10^{-9}\,\mathrm{m}^2\,\mathrm{s}^{-1}$ [102–104]
Cell volume fraction in viable epidermis and lower SC, ϕ_v	0.955±0.025 [36]	0.9925±0.0025 [40]
Ratio of the extracellular calcium distribution to its BM value, r	1.1±0.6 [33, 34]	1.25±0.75 [32]

Parameters used for the numerical solutions in this paper. Justification is provided in Text S1.

Supporting Information Legends

Text S1. Justification of parameter values.

Table S1. Semi-quantitative extracellular epidermal calcium distributions, determined using ion capture cytochemistry.

Figure 1.

(a) **Total Ca^{2+} Profile**
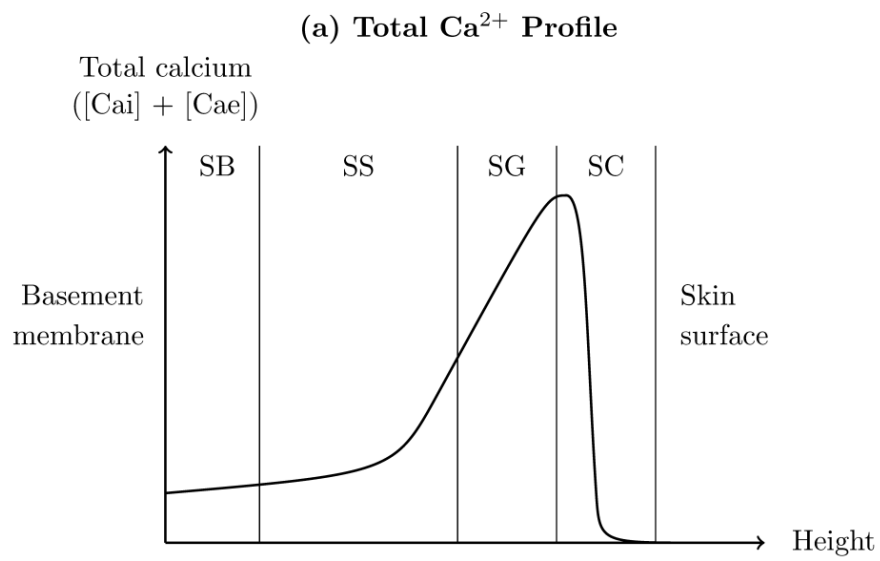
(b) **Intracellular and Extracellular Ca^{2+} Profiles**

	SB	SS	Lower SG	Upper SG	Lower SC	Upper SC
[Cai]	++/+++	+/+++	++/+++	++++	+/++	0/+
[Cae]	++	+/++	++/++++	+++/++++	+/++++	0/+

Figure 2.
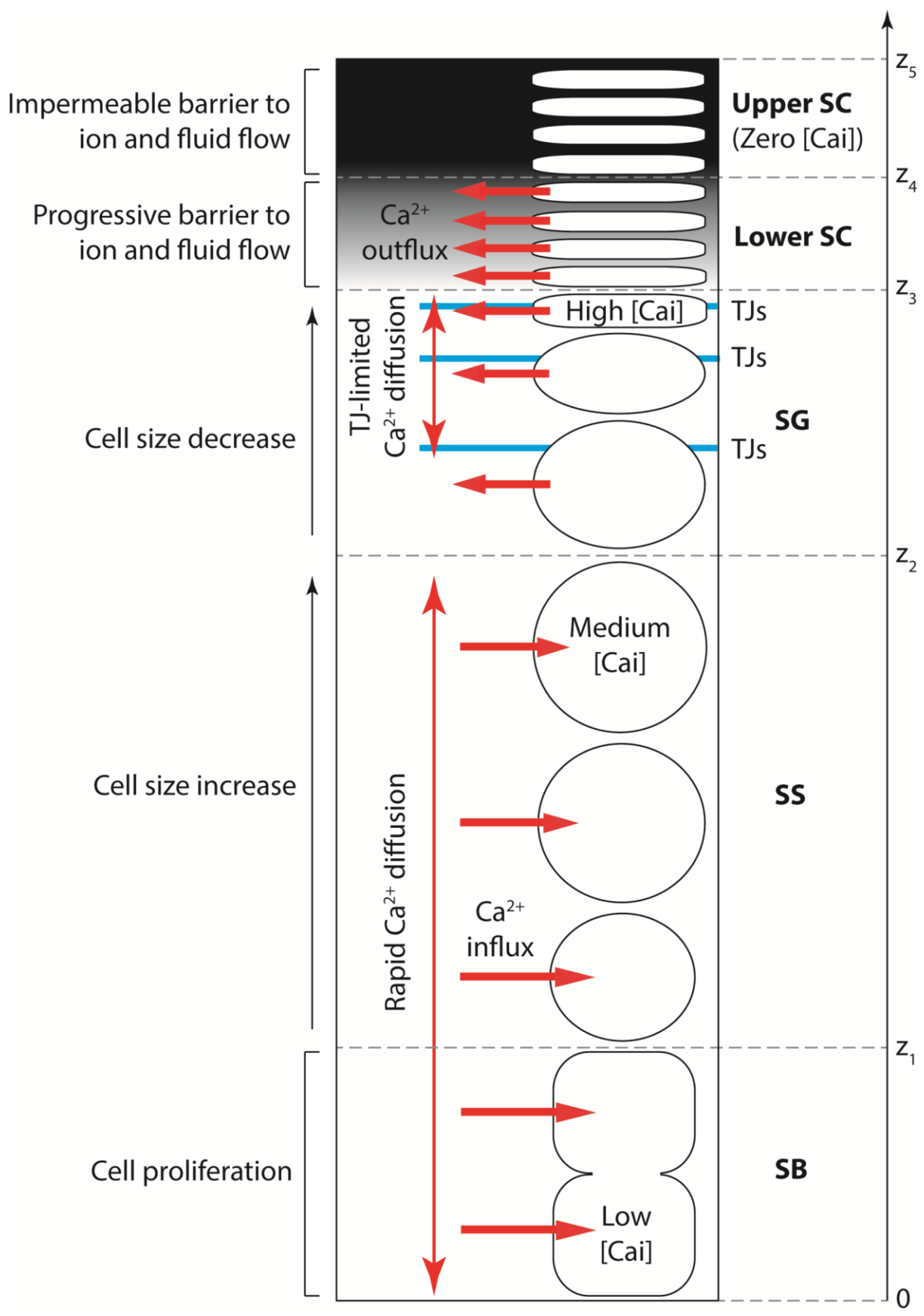
Figure 3.
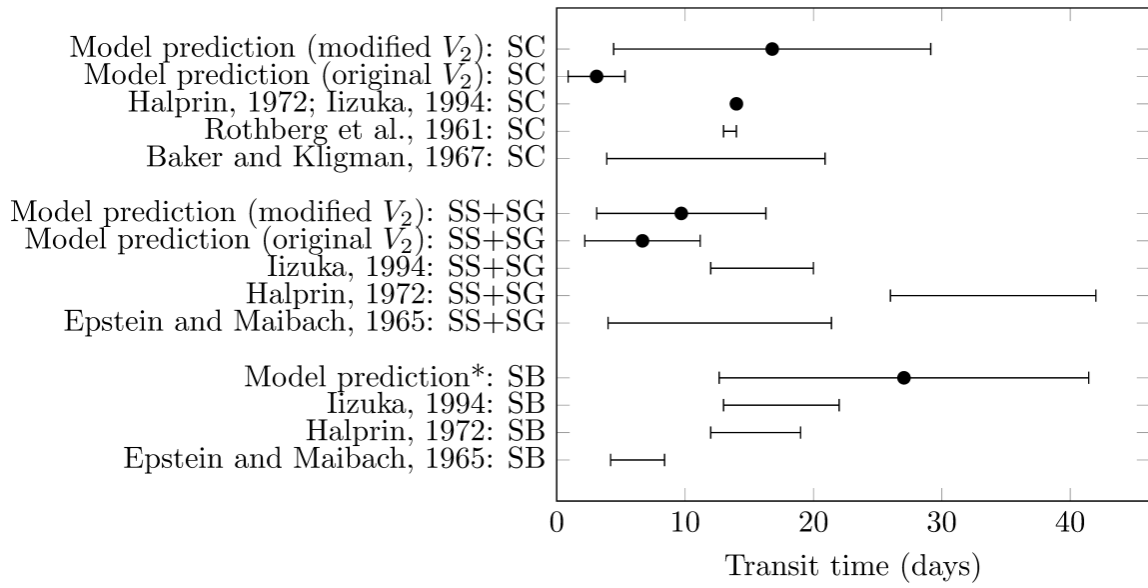
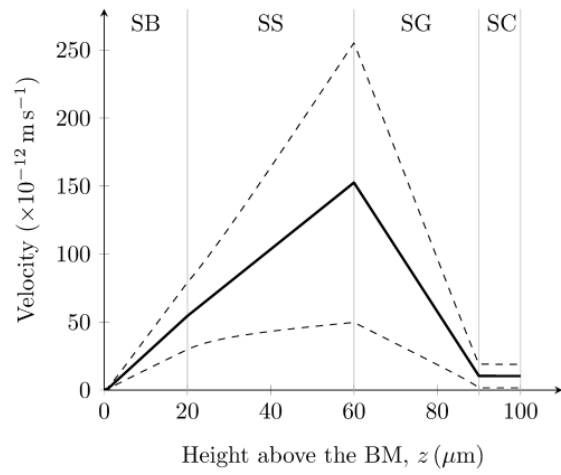(a) Transit times in human epidermis.
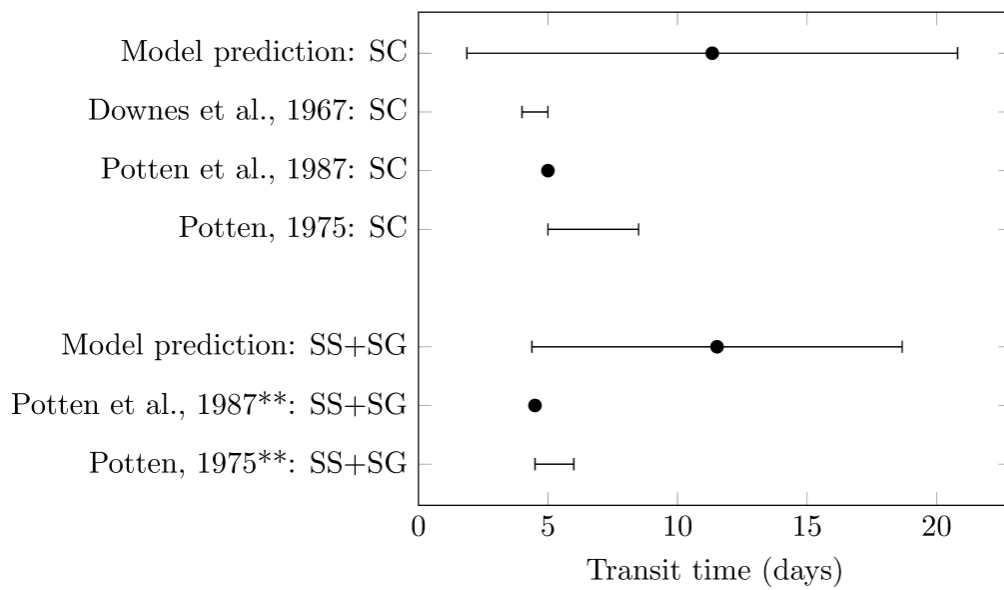
(b) Transit times in murine epidermis.
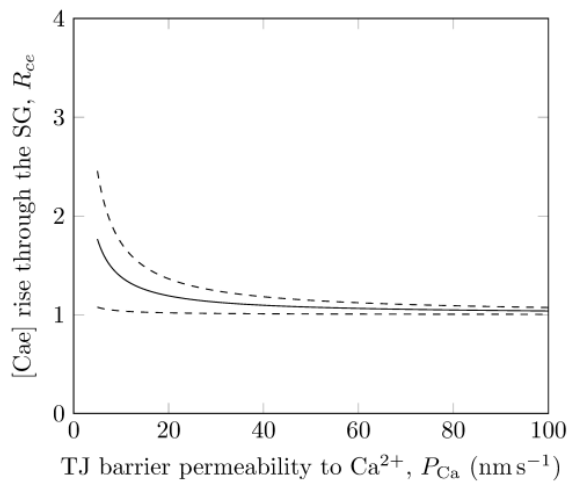
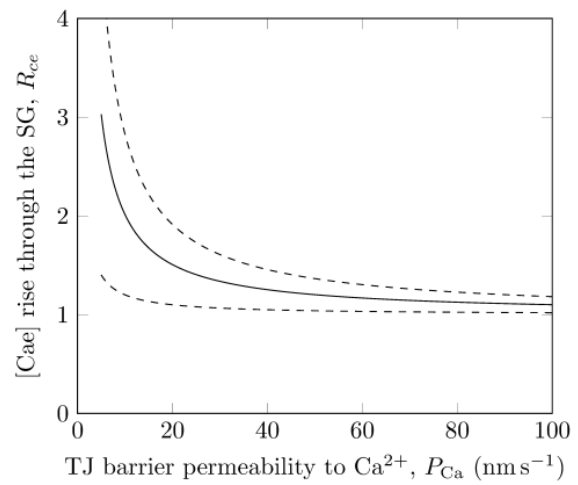**Figure 4.**
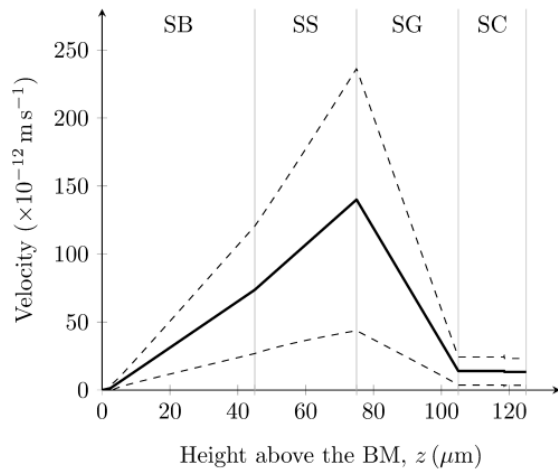
(a) Cell velocity in human epidermis.

(b) Cell velocity in murine epidermis.
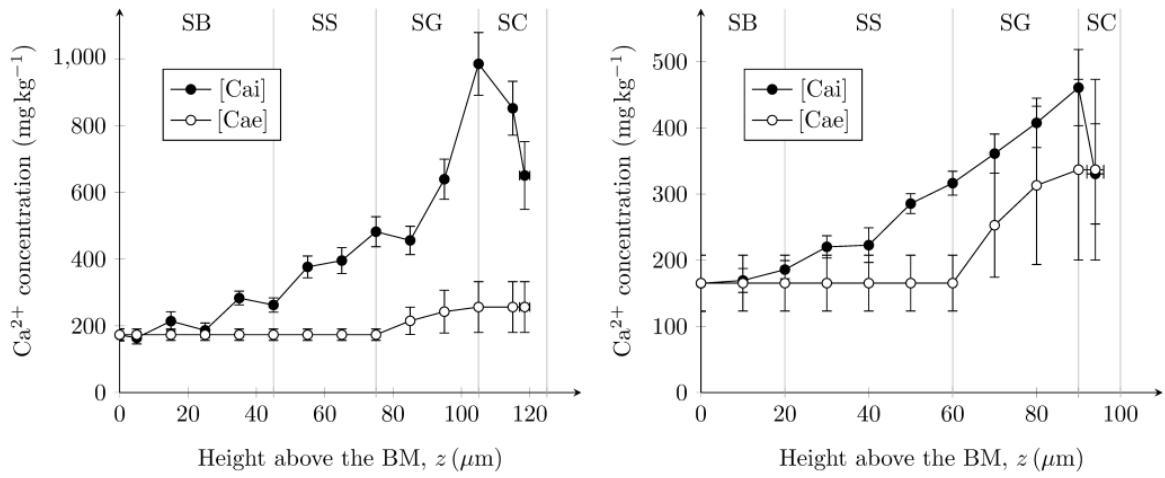
Figure 5.

(a) $R_{ce}(P_{Ca})$ in human epidermis.

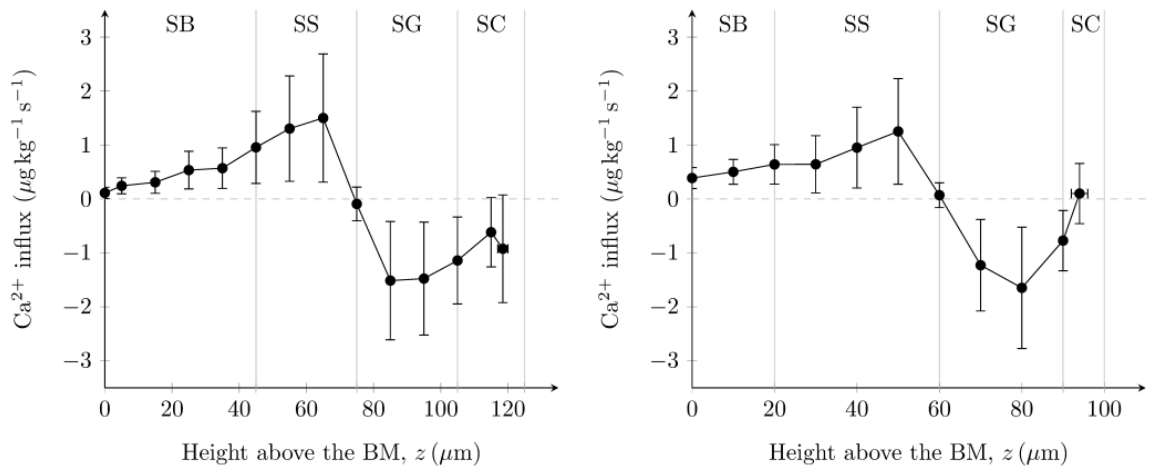(b) $R_{ce}(P_{Ca})$ in murine epidermis.

Figure 6.

(a) [Cai] and [Cae] in human epidermis.

(b) [Cai] and [Cae] in murine epidermis.

Figure 7.

(a) Cellular Ca^{2+} influx in human epidermis.

(b) Cellular Ca^{2+} influx in murine epidermis.

Text S1: Justification of Parameter Values

In the manuscript, Table 1 lists the parameters used in this paper and their key references. Here, we present the justification of the parameter values, starting from the experimental literature and applying subsequent calculations where necessary.

S.1 Stem cell volume fraction of the SB, θ

Li *et al.* state that epidermal stem cells constitute 1-10% of the SB based on several *in vivo* studies [1]. A range for the stem cell volume fraction of the SB that fully encompasses these estimates is $\theta = 0.055 \pm 0.045$. We assume that this value of θ applies to both human and murine epidermis.

S.2 Heights of the epidermal sublayer boundaries above the BM, z_1, z_2, z_3, z_4, z_5

For the human epidermal calcium profile investigated, the total epidermal thickness z_5 is $125\,\mu$m [2], and the thicknesses of the SB, SS, SG and SC are approximately 30-40 μm, 30 μm, 30 μm and 20 μm respectively, although the thickness of the SB is difficult to estimate due to undulation of the BM [3]. Hence we assume that the estimates of SS, SG and SC thickness are more accurate than the estimate of SB thickness, and consecutive subtraction of these values from $z_5 = 125\,\mu$m yields $z_3 = 105\,\mu$m, $z_2 = 75\,\mu$m and $z_1 = 45\,\mu$m.

For the estimation of z_4, we subtract from z_5 literature-reported estimates of the SC thickness removed at which transepidermal water loss (TEWL) becomes large. Bashir *et al.* reports that TEWL is significant after 5-7 μm of human SC is removed [4], whilst Kalia *et al.* reports that removal of $\sim$8 μm causes two- to ten-fold increase in TEWL [5]. We combine these values to estimate the thickness of upper SC in human epidermis as 6.5±1.5μm, and hence $z_4 = 118.5 \pm 1.5\,\mu$m.

For the murine epidermal calcium profile, all sublayer boundary heights are provided except z_4 [6]: $z_1 = 20\,\mu$m, $z_2 = 60\,\mu$m, $z_3 = 90\,\mu$m and $z_5 = 100\,\mu$m. In murine epidermis TEWL increases dramatically once 4-8 μm has been removed [7]. We therefore assume that the thickness of murine upper SC is 6±2 μm, and hence $z_4 = 94 \pm 2\,\mu$m.

S.3 Ratio of keratinocyte volumes SG:SB, V_1

For human epidermis, Bergstresser *et al.* reported the volumes of keratinocytes in basal and superficial layers, in six human subjects and three anatomical locations for each subject [8]. We assume that each of the 18 associated ratios of superficial to basal keratinocyte volume are a good approximation of the volume change of a keratinocyte during its passage through the SS. From the mean and standard deviation of these 18 ratios, we obtain $V_1 = 1.9 \pm 0.5$.

For murine epidermis, the volumes of keratinocytes in the basal and granular sublayers have been reported both by Rowden [9], and by Rodrigues and Maia Campos [10]. Ratios of granular to basal keratinocyte volume, calculated from these publications, are 4.2 and 1.4 respectively. We combine these values to obtain $V_1 = 2.8 \pm 1.4$.

S.4 Ratio of keratinocyte volumes SC:SG, V_2

For human epidermis, the original estimate of V_2 is based on the report of Norlén and Al-Amoudi that there is a reduction in cell volume between SG and SC keratinocytes from 700-900 μm^3 to 400-450 μm^3 [11], which corresponds to $V_2 = 0.54 \pm 0.10$. For murine epidermis, Allen and Potten report that mouse dorsum keratinocyte volume changes from 163 μm^3 at the SB to 31.1 μm^3 at the skin surface [12].

This corresponds to $V_1 \times V_2 = 0.1908$. Dividing this by our obtained value of murine $V_1 = 2.8 \pm 1.4$ yields $V_2 = 0.068 \pm 0.034$.

In our results we found that the estimate of human V_2 was questionable, due to its prediction of transit times through the SC that disagreed strongly with the experimental literature and its order of magnitude difference from the estimate of murine V_2 which predicted SC transit times that agreed more reasonably with the experimental literature. Hence, for the modified estimate of V_2 for human epidermis, we used the human $V_1 = 1.9 \pm 0.5$ obtained from [8] together with the murine $V_1 \times V_2 = 0.1908$ from [12] to obtain $V_1 = 0.100 \pm 0.026$.

S.5 Proliferation rate of stem cells in the SB, s_0

The stem cell cycle time is difficult to measure, but is suggested to be greater than 500 hours in human epidermis and approximately 200 hours in murine epidermis [13]. The stem cell proliferation rate can be obtained simply by inverting the cycle time. For simplicity we assume that the human and murine stem cycle times are equal to 500 hours and 200 hours respectively, and inversion immediately yields human $s_0 = 5.6 \times 10^{-7}\,\mathrm{s}^{-1}$ and murine $s_0 = 1.4 \times 10^{-6}\,\mathrm{s}^{-1}$.

S.6 Proliferation rate of TA cells in the SB, s_1

For both human and murine epidermis, the TA cell proliferation rate s_1 is calculated from literature-reported values of the mean proliferation rate in the SB, denoted here as s_μ, together with our found values for θ and s_0, via the equation

$$s_\mu = \theta s_0 + (1 - \theta)s_1. \tag{1}$$

For human epidermis, Castelijns *et al.* reported a mean cycle time of approximately $\sim$62.5 hours [14], which together with the growth fraction in the SB of 60% [15], yields an estimate of $s_\mu = 2.7 \times 10^{-6}\,\mathrm{s}^{-1}$. On the other hand, Iizuka reported that there are 27,000 cells and a birth rate of 1,246 cells per day in a $1\,\mathrm{mm}^2$ section of the proliferative compartment of human epidermis [15]. Dividing the birth rate by the number of cells yields an alternative estimate of $s_\mu = 5.3 \times 10^{-7}\,\mathrm{s}^{-1}$. Combining these two estimates, we choose $s_\mu = (1.6 \pm 1.1) \times 10^{-6}\,\mathrm{s}^{-1}$. Then, using equation (1) we obtain $s_1 = (1.7 \pm 1.1) \times 10^{-6}\,\mathrm{s}^{-1}$.

For murine epidermis, Potten reported that the cell production rate in murine epidermis varies from 0.55 to 1.42 cells per 100 basal cells per hour, depending on the anatomical location [16]. This corresponds to a mean proliferation rate in the SB of $s_\mu = (2.7 \pm 1.2) \times 10^{-6}\,\mathrm{s}^{-1}$. Then, using equation (1) we obtain $s_1 = (2.8 \pm 1.3) \times 10^{-6}\,\mathrm{s}^{-1}$.

S.7 Physical diffusion coefficient of calcium in the ECF, D_{Ca}

For both human and murine epidermis, we assume that the ECF is essentially water [17], and hence D_{Ca} is equal to the diffusion coefficient of calcium ions in water at skin temperature. We assume that the value of this diffusion coefficient is unaltered for the one-dimensional case, as our model considers only one spatial direction z perpendicular to the skin surface. The calculation of this coefficient from data in [18–20] together with the Stokes-Einstein equation [18] is detailed in Appendix A of our previous paper [21], and yields $D_{\mathrm{Ca}} = 1 \times 10^{-9}\,\mathrm{m}^{-2}\,\mathrm{s}^{-1}$.

S.8 Cell volume fraction in viable epidermis, ϕ_v

For human epidermis, Celli *et al.* reported that the cell volume fraction increases from 0.93 in the SB to 0.98 in the SG [22]. We combine these values to choose $\phi_v = 0.955 \pm 0.025$.

For murine epidermis, Elias and Leventhal reported that the ECF volume fraction, $1 - \phi_v$, is 0.5-1.0% in the SG [23]. We assume this value applies throughout the viable epidermis, and hence choose $\phi_v = 0.9925 \pm 0.0025$.

S.9   Ratio of the extracellular calcium distribution to its BM value, r

To calculate r for human and murine epidermis, we use data from the semi-quantitative extracellular calcium distributions shown in Table S1.

For human epidermis, we assume that the number of positive signs is proportional to the extracellular calcium level. From the use of this assumption on the data in [24] and [25], the mean extracellular calcium levels in human SB, SS, SG and lower SC are 2, 2, 2.75 and 2 (i.e. overall mean of 2.2), and the minimum and maximum reported extracellular calcium levels in the whole epidermis excluding the upper SC are 1 and 3 respectively. This data can be enclosed by an extracellular calcium level throughout the whole epidermis excluding the upper SC of 2.2±1.2, which written as a ratio of the mean extracellular calcium level in human SB, yields r =1.1±0.6.

For murine epidermis, we fit a five-point quantitative scale to the worded descriptors in [26]: 1 (very low), 2 (low), 3 (medium), 4 (high) and 5 (very high). Using this scale, the mean extracellular calcium levels in the SB, SS, SG and SC are 2, 1, 4 and 3 (i.e. overall mean of 2.5), and the minimum and maximum reported extracellular calcium levels in the whole epidermis excluding the upper SC are 1 and 4 respectively. This data can be enclosed by an extracellular calcium level throughout the whole epidermis excluding the upper SC of 2.5±1.5, which written as a ratio of the mean extracellular calcium level in murine SB, yields r =1.25±0.75.

References

1. Li A, Simmons P, Kaur P (1998) Identification and isolation of candidate human keratinocyte stem cells based on cell surface phenotype. P Natl Acad Sci USA 85: 3902-3907.

2. Behne M, Tu CL, Aronchik I, Epstein E, Bench G, et al. (2003) Human keratinocyte ATP2C1 localizes to the Golgi Ca^{2+} stores. J Invest Dermatol 121: 688-694.

3. Personal communications with T. M. Mauro and A. Celli (2013).

4. Bashir SJ, Chew AL, Anigbogu A, Dreher F, Maibach HI (2001) Physical and physiological effects of stratum corneum tape stripping. Skin Res Technol 7: 40-48.

5. Kalia YN, Alberti I, Sekkat N, Curdy C, Naik A, et al. (2000) Normalization of stratum corneum barrier function and transepidermal water loss *in vivo*. Pharm Res 17: 1148-1150.

6. Mauro T, Bench G, Sidderas-Haddad E, Feingold K, Elias P, et al. (1998) Acute barrier perturbation abolishes the Ca^{2+} and K^+ gradients in murine epidermis: quantitative measurement using PIXE. J Invest Dermatol 111: 1198-1201.

7. Yow HN, Wu X, Routh AF, Guy RH (2009) Dye diffusion from microcapsules with different shell thickness into mammalian skin. Eur J Pharm Biopharm 72: 62-68.

8. Bergstresser PR, Pariser RJ, Taylor JR (1978) Counting and sizing of epidermal cells in normal human skin. J Invest Dermatol 70: 280-284.

9. Rowden G (1975) Ultrastructural studies of keratinized epithelia of the mouse. III. Determination of the volumes of nuclei and cytoplasm of cells in murine epidermis. J Invest Dermatol 64: 1-3.

10. Rodrigues LHT, Maia Campos PMBG (2002) Comparative study of the effects of cosmetic formulations with or without hydroxy acids on hairless mouse epidermis by histopathologic, morphometric, and stereologic evaluation. J Cosmet Sci 53: 269-282.

11. Norlén L, Al-Amoudi A (2004) Stratum corneum keratin structure, function, and formation: the cubic rod-packing and membrane templating model. J Invest Dermatol 123: 715-732.

12. Allen T, Potten C (1976) Ultrastructural site variations in mouse epidermal organization. J Cell Sci 21: 341-359.

13. Potten C, Booth C (2002) Keratinocyte stem cells: a commentary. J Invest Dermatol 119: 888-899.

14. Castelijns F, Ezendam J, Latijnhouwers M, Vlijmen-Willems IV, Zeeuwen P, et al. (1998) Epidermal cell kinetics by combining *in situ* hybridization and immunohistochemistry. Histochem J 30: 869-877.

15. Iizuka H (1994) Epidermal turnover time. J Dermatol Sci 8: 215-217.

16. Potten C (1975) Epidermal cell production rates. J Invest Dermatol 65: 488-500.

17. Halprin K, Ohkawara A (1967) Glucose entry into the human epidermis: II. The penetration of glucose into the human epidermis *in vitro*. J Invest Dermatol 49: 561-568.

18. Li YH, Gregory S (1974) Diffusion of ions in sea water and in deep-sea sediments. Geochim Cosmochim Ac 38: 703-714.

19. Kampmeyer P (1952) The temperature dependence of viscosity for water and mercury. J Appl Phys 23: 99-102.

20. Williams E, Heusch A, McCarthy P (2008) Thermal screening of facial skin arterial hot spots using non-contact infrared radiometry. Physiol Meas 29: 341-348.

21. Adams MP, Mallet DG, Pettet GJ (2012) Active regulation of the epidermal calcium profile. J Theor Biol 301: 112-121.

22. Celli A, Sanchez S, Behne M, Hazlett T, Gratton E, et al. (2010) The epidermal Ca^{2+} gradient: measurement using the phasor representation of fluorescent lifetime imaging. Biophys J 98: 911-921.

23. Elias P, Leventhal M (1979) Intercellular volume changes and cell surface expansion during cornification. Clin Res 27: 525A.

24. Menon G, Elias P (1991) Ultrastructural localization of calcium in psoriatic and normal human epidermis. Arch Dermatol 127: 57-63.

25. Vičanová J, Boelsma E, Mommaas A, Kempenaar J, Forslind B, et al. (1998) Normalization of epidermal calcium distribution profile in reconstructed human epidermis is related to improvement of terminal differentiation and stratum corneum barrier formation. J Invest Dermatol 111: 97-106.

26. Menon G, Grayson S, Elias P (1985) Ionic calcium reservoirs in mammalian epidermis: Ultrastructural localization by ion-capture cytochemistry. J Invest Dermatol 84: 508-512.

Table S1. Semi-quantitative extracellular epidermal calcium distributions, determined using ion capture cytochemistry

Extracellular Calcium Concentration						Species, Reference
SB	**SS**	**Lower SG**	**Upper SG**	**Lower SC**	**Upper SC**	
++	++	+++	+++	+++	0	Human, [1]
++	++	++	+++	+	0	Human, [2]
Low	Very low	High	High	High-Low	Low	Mouse, [3]

References

1. Menon G, Elias P (1991) Ultrastructural localization of calcium in psoriatic and normal human epidermis. Arch Dermatol 127: 57-63.

2. Vičanová J, Boelsma E, Mommaas A, Kempenaar J, Forslind B, et al. (1998) Normalization of epidermal calcium distribution profile in reconstructed human epidermis is related to improvement of terminal differentiation and stratum corneum barrier formation. J Invest Dermatol 111: 97-106.

3. Menon G, Grayson S, Elias P (1985) Ionic calcium reservoirs in mammalian epidermis: Ultrastructural localization by ion-capture cytochemistry. J Invest Dermatol 84: 508-512.